Valley and band structure engineering of folded MoS$_2$ bilayers

Tao Jiang[1,2], Hengrui Liu[1,3], Di Huang[1,2], Shuai Zhang[1,2], Yingguo Li[1,2], Xingao Gong[1,3,4]★, Yuen-Ron Shen[1,2,5], Wei-Tao Liu[1,2,4]★ and Shiwei Wu[1,2,4]★

Artificial structures made of stacked two-dimensional crystals have recently been the focus of intense research activity[1]. As in twisted or stacked graphene layers[2–6], these structures can show unusual behaviours and new phenomena[1]. Among the various layered compounds that can be exfoliated, transition-metal dichalcogenides[7] exhibit interesting properties governed by their structural symmetry[8,9] and interlayer coupling[10–13], which are highly susceptible to stacking. Here, we obtain—by folding exfoliated MoS$_2$ monolayers—MoS$_2$ bilayers with different stacking orders, as monitored by second harmonic generation and photoluminescence. Appropriate folding can break the inversion symmetry and suppress interlayer hopping, evoking strong valley[14–16] and spin[17–19] polarizations that are not achieved in natural MoS$_2$ bilayers of Bernal stacking[20]. It can also enlarge the indirect bandgap by more than 100 meV through a decrease in the interlayer coupling. Our work provides an effective and versatile means to engineer transition-metal dichalcogenide materials with desirable electronic and optical properties.

Monolayers of group VI transition-metal dichalcogenides (TMDCs) MX$_2$ (M = Mo, W; X = S, Se, Te) are composed of X–M–X unit cells that have a hexagonal honeycomb structure similar to that of graphene, but with M and X located at alternate corners of the hexagon[7]. This breaks the inversion symmetry in the monolayer. Because it has electrons from transition-metal ions with strong spin–orbit coupling (SOC), the monolayer exhibits extraordinary valley-contrasting physics[8,9,14–16,20]. In bilayers, the interlayer coupling, depending on the relative atomic positions of one layer with respect to the other, modifies the band structure and causes a direct-to-indirect bandgap transition[10–13]. To control the physical properties of TMDCs and enable applications in valleytronics and optoelectronics[7–9], techniques such as electric bias[20], strain[21] and chemical doping[22,23] have been applied. However, the two-dimensional nature of layered compounds provides a unique opportunity to engineer their properties at the atomic level by stacking monolayers in different ways[1]. Indeed, such an approach has already been applied to graphene and has generated exciting results, such as Hofstadter's spectra[2–4] and the emergence of Van Hove singularities[5,6]. We expect this stacking to have a similarly pronounced impact on TMDCs, as their behaviours are dominated by structural symmetry and interlayer coupling.

In the present experiment, stacked MoS$_2$ layers were obtained by folding exfoliated monolayers like origami. A white-light microscopic image of exfoliated MoS$_2$ (Fig. 1a) shows that the sample consists predominantly of a monolayer sheet (1L) with a trilayer (3L) on the right side. As shown in Fig. 1b, the photoluminescence spectrum

of the monolayer is dominated by the A-exciton transition at ~1.89 eV, while the trilayer photoluminescence spectrum has an additional peak at ~1.43 eV from the indirect-gap transition[10–12].
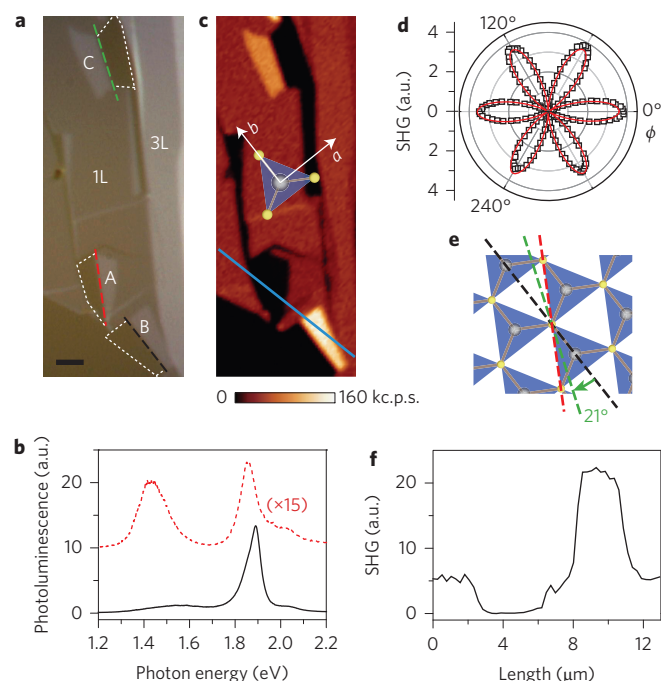

Figure 1 | Microscopy and characterization of monolayer, folded bilayers, and trilayer of MoS$_2$. a, White-light microscope image of the MoS$_2$ sample. 1L and 3L refer to the monolayer and trilayer, respectively. A, B and C are folded bilayers, with folding edges highlighted by dashed red, black and green lines, respectively. Their mirror shapes are marked by dotted frames on the monolayer sheet. Scale bar: 2 μm. **b**, Photoluminescence spectra of 1L (solid black) and 3L (dashed red) (magnified ×15) in **a**, excited at 2.33 eV. Spectra are shifted vertically for clarity. **c**, Second harmonic generation (SHG) microscope images of the same region in **a**, with the fundamental input beam at 900 nm. The monolayer lattice coordinates (*a* and *b*, *b* ∥ a mirror plane) are shown with a MoS$_2$ unit cell, with yellow and grey balls indicating sulphur and molybdenum atoms, respectively. The colour map represents the SHG intensity from 0 to 1.6 × 10^5 counts per second. **d**, SHG anisotropy pattern of 1L, where ϕ is the angle between the *b*-axis and polarizations of both input and output beams. The red solid line is a fit to data points (black open squares). **e**, Folding orientations of bilayers A, B and C with respect to the 1L lattice, marked by dashed red, black and green lines, respectively. **f**, SHG intensity profile along the blue line-cut in **c**.
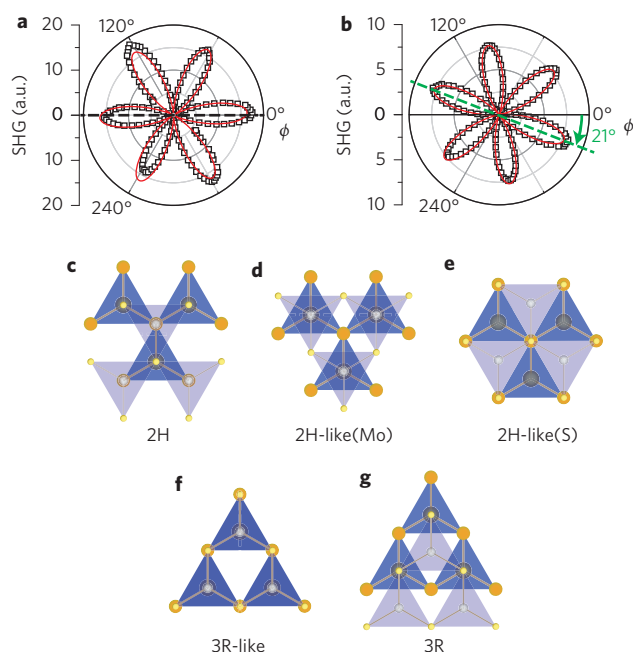
Figure 2 | Second harmonic generation (SHG) anisotropy and microscopic structures of folded MoS$_2$ bilayers. a,b, SHG anisotropy patterns of bilayers B and C, respectively, where ϕ is the angle between the light polarization and the b-axis of the monolayer in Fig. 1. Red solid lines are fits to data points (black open squares). Black and green dashed lines mark the folding orientations as in Fig. 1e. **c–g**, Top views of atomic structures of the 2H, 2H-like(Mo), 2H-like(S), 3R-like and 3R bilayers, respectively. Top layers are represented by lighter triangles and smaller atoms. The top and bottom lattices of the 3R-like bilayer (**f**) coincide completely. Except for the 3R structure, all these structures can be obtained directly from folding of the monolayer.

There are also stripes, labelled A, B and C in Fig. 1a, that can be identified as bilayers. As can be seen from their contrasted mirror shapes (dotted frames in Fig. 1a) on the monolayer sheet, the bilayers were formed by folding (the edges are highlighted by dashed lines).

To find the structure and orientation of the bilayers we first need to identify the orientation of the native monolayer. This can be accomplished by measuring second harmonic generation (SHG) from the monolayer as a function of its azimuthal position. The principle of SHG from MoS$_2$ is described in the Supplementary Section 1. Briefly, monolayer MoS$_2$ belongs to the non-centrosymmetric point group D_{3h} (ref. 24). If the input and output have the same polarization, parallel to the monolayer surface, the SHG output from the monolayer is proportional to $|\chi_{bbb}^{(2)}|^2 \cos^2 3\phi$, where $\chi_{bbb}^{(2)}$ is the responsible nonlinear susceptibility element of MoS$_2$, b denotes the crystalline axis along a mirror plane[25] (Fig. 1c), and ϕ is the angle of the beam polarization away from the b-axis[26–29]. The result presented in Fig. 1d shows a six-fold pattern, with maxima appearing when the polarization lies in a mirror plane. By knowing how the beam polarization is aligned with respect to the monolayer we can readily determine the orientation of the monolayer lattice (a sketch of a unit cell is shown in Fig. 1d). We can then directly measure the angle ϕ_f between a folding edge and the indicated b-axis from the microscopic image (Fig. 1c). We find ϕ_f equal to 30°, 0° and 21° for bilayers A, B and C, respectively (Fig. 1e).

In contrast to natural bilayers of Bernal stacking, which yield no SHG[26–29], the SHG from folded bilayers is stacking-dependent (Fig. 1f), which is consistent with the folding angles measured above. The folding line of bilayer A is perpendicular to the mirror
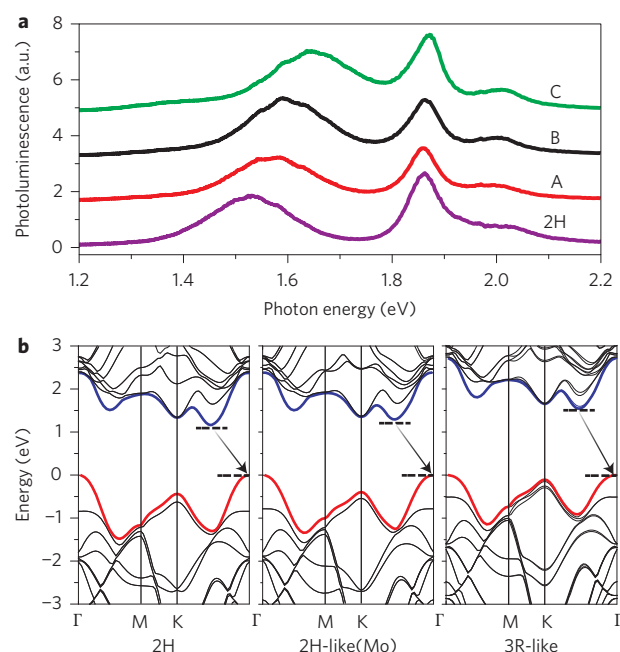
Figure 3 | Photoluminescence spectra and band structures of MoS$_2$ bilayers with different stacking orders. a, Photoluminescence spectra excited at 2.33 eV of the natural 2H bilayer (purple), bilayer A (red), bilayer B (black) and bilayer C (green). Spectra are shifted vertically for clarity. **b**, Left to right: band structures of 2H, 2H-like(Mo) and 3R-like bilayers by *ab initio* calculations with spin–orbit coupling. The lowest conduction band and highest valence band are highlighted in blue and red, respectively. Arrows mark the corresponding indirect-gap transitions.

plane, which creates an inversion centre between the top and bottom layers, causing the vanishing SHG. When the folding line is not perpendicular to the mirror plane, as for bilayers B and C, the inversion symmetry will be explicitly broken, leading to non-zero SHG. Moreover, provided that there is no reorientation between the top and bottom layers after folding, the resultant bilayer will have a two-fold symmetry axis parallel to the folding line. This causes the SHG to reach a maximum when the beam polarization is aligned with the folding line (for detailed derivation see Supplementary Section 2) and indeed this is what we observe for bilayers B and C (Fig. 2a,b).

With the relative orientation between top and bottom layers confirmed by SHG, we can further deduce the bilayer atomic structures. For bilayer A there are three possible structures, which are local energy minima according to our *ab initio* calculation. One is identical to the natural MoS$_2$ bilayer with Bernal stacking (2H; Fig. 2c) and the other two have Mo (S) of the two layers on top of each other (labelled 2H-like(Mo) and 2H-like(S) in Fig. 2d,e). To determine which of the three possible structures bilayer A assumes, we rely on photoluminescence measurements, as discussed later. For bilayer B, the SHG anisotropy is six-fold symmetric. This indicates that bilayer B must be three-fold symmetric and the only possible structure for it is with two monolayers stacked with atoms in identical positions, as illustrated in Fig. 2f. It differs from the natural rhombohedral (3R) bilayer structure[7] (Fig. 2g) by a gliding between the top and bottom layers along the folding line, so we call bilayer B '3R-like'. The *ab initio* calculation confirms it to be a local energy minimum. Moreover, the 3R-like bilayer is effectively a 'doubled monolayer'. So, its nonlinear susceptibility, and therefore the maximum SHG signal, are respectively two and four times those of a monolayer, as we observed. For bilayer C, it exhibits a moiré pattern, as sketched in Supplementary Fig. 2.
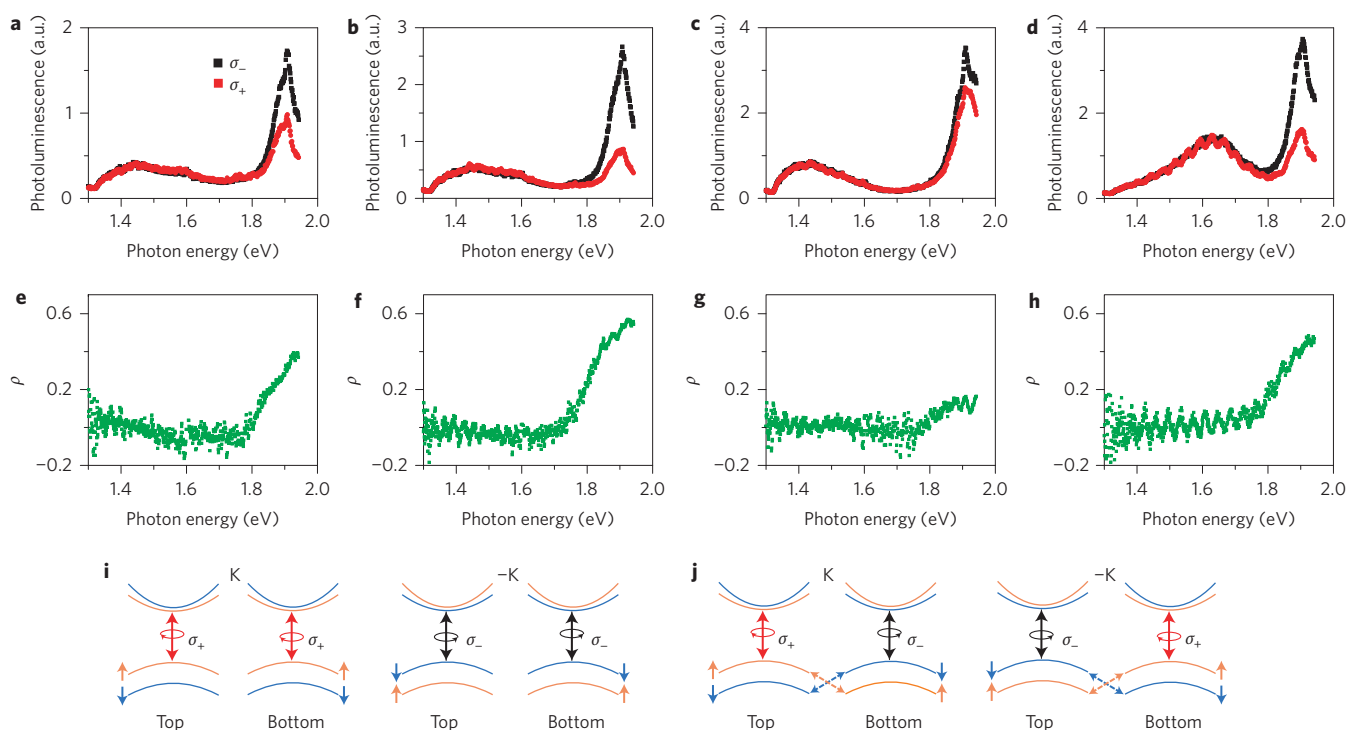
Figure 4 | Valley and spin polarizations in 2H-like(Mo), 3R-like and 2H bilayers. a–d, Circularly polarized photoluminescence spectra from 2H-like(Mo) bilayer A, 3R-like bilayer B, natural 2H bilayer and monolayer, respectively. Excitation light is left-circularly polarized at 1.96 eV. Left- (σ_-) and right- (σ_+) circularly polarized photoluminescence spectra are shown in black and red. **e–h**, Helicity parameters calculated from photoluminescence spectra in **a–d** for 2H-like(Mo) bilayer, 3R-like bilayer, natural 2H bilayer and monolayer, respectively. **i,j**, Schematic depictions of circularly polarized-light-excited valley and spin polarizations in 3R-like bilayers, and spin polarization in 2H and 2H-like bilayers, respectively. The spin-up and -down bands at K/–K valleys and top/bottom layers are marked in orange and blue, respectively. The A-exciton transitions excited by left- (σ_-, black) or right- (σ_+, red) circularly polarized light are marked by vertical arrows across the bandgap. The interlayer hopping of holes is indicated by dotted arrows.

Besides symmetry, the stacking order also modulates the interlayer coupling and hence the band structure of bilayer MoS_2 (refs 10–13). Figure 3a presents photoluminescence spectra of the natural 2H bilayer, and folded bilayers A, B and C. The A exciton at ~1.86 eV shifts by only ~10 meV, but the indirect-gap transition near 1.6 eV varies notably by ~120 meV. The A-exciton transition is between the states of strongly localized Mo-d orbitals that have little interlayer overlapping and are hardly affected by the stacking[10]. The indirect-gap transition, however, occurs between the conduction band minimum halfway on the K-Γ line and the valence band maximum at the Γ point, and states near these band extrema originate from linear combinations of Mo-d and S-p orbitals[10]. As these orbitals have strong interlayer overlapping, the indirect-gap energy is highly sensitive to the stacking order[10–13]. Comparing the structures in Fig. 2c–g, Mo and S atoms from opposite layers sit on top of each other in both natural 2H and 3R crystals, but are staggered in the other structures. So, the interlayer coupling must be strongest in natural bilayers. Among the others, 2H-like(S) and 3R-like bilayers have negatively charged S atoms stacked directly on top of each other. By Coulomb repulsion, their interlayer spacing is enlarged and the coupling is reduced. Accordingly, we expect the strength of interlayer coupling to be 3R ≈ 2H > 2H-like(Mo) > 2H-like(S) ≈ 3R-like. The indirect gap is expected to follow a reverse order because it is known to decrease with increasing interlayer coupling[10], as confirmed by our *ab initio* calculations (described in the Supplementary Section 3). From our observed sequence that 2H (1.53 eV) < bilayer A (1.57 eV) < bilayer B (1.60 eV), the most probable structure of bilayer A is 2H-like(Mo), because it is distinct from both 2H and 3R-like bilayers. The computed band structures with SOC of the natural 2H bilayer, 2H-like(Mo) and 3R-like bilayers are presented in Fig. 3b.

We now discuss the photoluminescence spectrum of bilayer C, which exhibits a moiré pattern with Mo and S atoms alternately stacked on top of each other. The interlayer spacing is then expected to be an average of the values for the 2H and 3R-like bilayers, as would also be the case for the indirect-gap energy. However, the observed indirect-gap transition of C (1.65 eV) is even higher than that of the 3R-like bilayer (1.60 eV). This is because the moiré pattern also leads to zone folding[6,30,31]. As for twisted bilayer graphene, the density of states of bilayer C is redistributed and can cause the observed transition energy to increase. This suggests that the tuning range of the indirect-gap energy by folding is at least 120 meV if the stacking order can be varied controllably, as demonstrated for graphene in ref. 32.

As discussed already, certain stacking orders can break the inversion symmetry and reduce the interlayer coupling, which are prerequisites for valley- and/or spin-selective circular dichroism, respectivley[8,9,17]. Figure 4a–d shows the circularly polarized photoluminescence spectra from folded bilayers A and B, exfoliated natural 2H bilayer and monolayer, with $\sigma_{-/+}$ denoting the left-/right-circular polarization. The σ_--polarized excitation light at 1.96 eV is near the A exiton[14]. Figure 4e–h shows the corresponding helicity parameter, $\rho = [I(\sigma_-) - I(\sigma_+)]/[I(\sigma_-) + I(\sigma_+)]$, determined from the circularly polarized photoluminescence intensities $I(\sigma_{-/+})$[14,20]. The 2H bilayer has a small ρ of ~10% for the A exciton, which is typical for substrate-supported samples and indicates a negligible valley or spin polarization[14,20]. In contrast, ρ of the 2H-like(Mo) bilayer A and 3R-like bilayer B is greatly enhanced to ~40% and ~60% for the A exciton, comparable to the value of ~50% in the monolayer[14–16] and far exceeding the value achieved in electrically gated 2H bilayers[20].

The enhanced ρ is expected for the 3R-like bilayer B, as it is a 'doubled monolayer'. Like in the monolayer, the spin and valley

degrees of freedom are locked in bilayer B due to the broken inversion symmetry (Fig. 4i), yielding strong circular dichroism that is both spin- and valley-selective[8,9]. This is also the case for bilayer C, as shown in Supplementary Fig. 3. The centrosymmetric 2H-like (Mo) bilayer A has no valley-selective circular dichroism[8,9,14–17], yet still exhibits a large value of ρ. This is because the spin-selective circular dichroism can persist, provided that interlayer hopping is small[17]. As shown in Fig. 4j, the spin configuration in a given valley depends on the layer index for both 2H and 2H-like bilayers[17]. In natural 2H bilayers, the interlayer hopping amplitude of holes is comparable to the SOC strength[17], which mixes the layer pseudospins and suppresses the overall spin polarization. In folded bilayers, however, interlayer coupling can be largely reduced as discussed above, so the spin configuration becomes locked to the layer index, leading to the observed circular dichroism. Similar phenomena have been reported recently in natural 2H bilayers of WSe_2 (ref. 18) and WS_2 (ref. 19), where the interlayer hopping is quenched by the large SOC in Wd-orbitals[17].

In summary, we have shown, with SHG, photoluminescence and *ab initio* calculation, that folding of a MoS_2 monolayer can produce bilayers of various stacking orders that are resolvable microscopically and lead to different optical nonlinearities, indirect-gap energies, and valley- and/or spin-selective circular dichroism. This provides a feasible means with which to obtain artificial MoS_2 bilayers, and TMDC bilayers in general, of desired properties in a simple way. Such an approach can open up a new route for fundamental research on TMDCs and electronic and optoelectronic applications.

Methods

Sample preparation. Monolayer, bilayer and trilayer MoS_2 samples a few tens of micrometres in size were obtained by mechanical exfoliation from a 2H-MoS_2 bulk crystal (SPI). The substrate was an elastic polyethylene terephthalate (PET) film covered by silica gel, which gives a high yield of folded samples.

Optical measurements. For photoluminescence measurements a HeNe laser (1.96 eV) was used for excitation in circularly polarized photoluminescence measurements, and a solid-state laser at 2.33 eV was used otherwise. To achieve circularly polarized excitation, a liquid-crystal retarder (Thorlabs, LCR-1-VIS) was used and the state of circular polarization was confirmed at the sample location. The laser beams were focused on the sample at normal incidence using an objective (Nikon, ×50/NA0.45), which also collected the emitted photoluminescence in the reflected direction. For circularly polarized photoluminescence, a laser power of 55 μW was used before the objective, corresponding to ~4 kW cm^{-2} power density at the sample. The sample was kept at 12 K for circularly polarized photoluminescence measurements, or at room temperature otherwise. The emitted photoluminescence was sent through an achromatic quarter-wave Fresnel rhomb (Thorlabs, FR600QM) followed by a linear polarizer in the circularly polarized photoluminescence measurements. The photoluminescence then passed through a 5-m-long depolarizing multimode optical fibre (100/140 μm, NA = 0.22) to a spectrograph equipped with a silicon charge-coupled device (Princeton Instruments, Spec-10:100BR/LN_eXcelon).

For SHG measurements, the 900 nm output from a 80 MHz Ti:sapphire oscillator (Spectra-Physics, MaiTai HP) was used as the fundamental input in SHG measurements. The laser beam was sent through a linear polarizer followed by a half-wave plate to rotate its polarization, then focused on the sample at normal incidence using an objective (Nikon, ×100/NA0.95), which also collected the emitted SHG signal in the reflected direction. The microscopic images were taken with a piezo-driven sample stage. The SHG signals then passed through a beamsplitter and a linear polarizer. The anisotropy pattern was corrected using a z-cut quartz[33] and detected in the same fashion. The integrated SHG signals were finally collected by a single photon-counting silicon avalanche photodiode. Details of the optical layouts are provided in the Supplementary Section 5.

***Ab initio* calculations.** The structural and electronic properties of bulk and bilayer MoS_2 were calculated using density functional theory, implemented in VASP code. For the exchange-correlation potential we used the local density approximation, and the contribution from SOC was also included. The projector-augmented-wave pseudopotential with an energy cutoff of 400 eV for the plane-wave basis sets was adopted, and gamma-centred $11 \times 11 \times 3$ and $11 \times 11 \times 1$ Monkhorst–Pack k-point meshes were used to achieve converged results for bulk and bilayer slab calculations, respectively. All atomic positions and lattice constants were optimized in bulk calculations by using the conjugate gradient method, with the total energy and atomic forces minimized. For bilayer slabs, the lattice constants in the a–b plane were fixed at their bulk values while all atomic positions were fully relaxed, and a vacuum region of ~15 Å was applied along the z-direction, which is large enough to make the mirror interaction between neighbouring images negligible. The convergence for total energy was chosen to be less than 1×10^{-5} eV between two consecutive steps, and the maximum Hellmann–Feynman forces acting on each atom were less than 0.02 eV Å^{-1} upon ionic relaxation.

References

1. Geim, A. K. & Grigorieva, I. V. Van der Waals heterostructures. *Nature* **499**, 419–425 (2013).
2. Dean, C. R. *et al.* Hofstadter's butterfly and the fractal quantum Hall effect in moiré superlattices. *Nature* **497**, 598–602 (2013).
3. Ponomarenko, L. A. *et al.* Cloning of Dirac fermions in graphene superlattices. *Nature* **497**, 594–597 (2013).
4. Hunt, B. *et al.* Massive Dirac fermions and Hofstadter butterfly in a Van der Waals heterostructure. *Science* **340**, 1427–1430 (2013).
5. Li, G. *et al.* Observation of Van Hove singularities in twisted graphene layers. *Nature Phys.* **6**, 109–113 (2010).
6. Kim, K. *et al.* Raman spectroscopy study of rotated double-layer graphene: misorientation-angle dependence of electronic structure. *Phys. Rev. Lett.* **108**, 246103 (2012).
7. Wang, Q. H. *et al.* Electronics and optoelectronics of two-dimensional transition metal dichalcogenides. *Nature Nanotech.* **7**, 699–712 (2012).
8. Xiao, D., Liu, G-B., Feng, W., Xu, X. & Yao, W. Coupled spin and valley physics in monolayers of MoS_2 and other group-VI dichalcogenides. *Phys. Rev. Lett.* **108**, 196802 (2012).
9. Yao, W., Xiao, D. & Niu, Q. Valley-dependent optoelectronics from inversion symmetry breaking. *Phys. Rev. B* **77**, 235406 (2008).
10. Splendiani, A. *et al.* Emerging photoluminescence in monolayer MoS_2. *Nano Lett.* **10**, 1271–1275 (2010).
11. Mak, K. F., Lee, C., Hone, J., Shan, J. & Heinz, T. F. Atomically thin MoS_2: a new direct-gap semiconductor. *Phys. Rev. Lett.* **105**, 136805 (2010).
12. Zhao, W. *et al.* Origin of indirect optical transitions in few-layer MoS_2, WS_2 and WSe_2. *Nano Lett.* **13**, 5627–5634 (2013).
13. Zhang, Y. *et al.* Direct observation of the transition from indirect to direct bandgap in atomically thin epitaxial $MoSe_2$. *Nature Nanotech.* **9**, 111–115 (2014).
14. Mak, K. F., He, K., Shan, J. & Heinz, T. F. Control of valley polarization in monolayer MoS_2 by optical helicity. *Nature Nanotech.* **7**, 494–498 (2012).
15. Zeng, H., Dai, J., Yao, W., Xiao, D. & Cui, X. Valley polarization in MoS_2 monolayers by optical pumping. *Nature Nanotech.* **7**, 490–493 (2012).
16. Cao, T. *et al.* Valley-selective circular dichroism of monolayer molybdenum disulphide. *Nature Commun.* **3**, 887 (2012).
17. Gong, Z. *et al.* Magnetoelectric effects and valley-controlled spin quantum gates in transition metal dichalcogenide bilayers. *Nature Commun.* **4**, 2053 (2013).
18. Jones, A. M. *et al.* Spin-layer locking effects in optical orientation of exciton spin in bilayer WSe_2. *Nature Phys.* **10**, 130–134 (2014).
19. Zhu, B., Zeng, H., Dai, J., Gong, Z. & Cui, X. Anomalous robust valley polarization and valley coherence in bilayer WS_2. Preprint at http://arxiv.org/abs/1403.6224 (2014).
20. Wu, S. *et al.* Electrical tuning of valley magnetic moment through symmetry control in bilayer MoS_2. *Nature Phys.* **9**, 149–153 (2013).
21. He, K., Poole, C., Mak, K. F. & Shan, J. Experimental demonstration of continuous electronic structure tuning via strain in atomically thin MoS_2. *Nano Lett.* **13**, 2931–2936 (2013).
22. Gong, Y. *et al.* Band gap engineering and layer-by-layer mapping of selenium-doped molybdenum disulfide. *Nano Lett.* **14**, 442–449 (2014).
23. Mann, J. *et al.* 2-Dimensional transition metal dichalcogenides with tunable direct band gaps: $MoS_{2(1-x)}Se_{2x}$ monolayers. *Adv. Mater.* **26**, 1399–1404 (2014).
24. Molina-Sanchez, A. & Wirtz, L. Phonons in single-layer and few-layer MoS_2 and WS_2. *Phys. Rev. B* **84**, 155413 (2011).
25. Shen, Y. R. *The Principles of Nonlinear Optics* 27 (Wiley, 2003).
26. Li, Y. *et al.* Probing symmetry properties of few-layer MoS_2 and h-BN by optical second-harmonic generation. *Nano Lett.* **13**, 3329–3333 (2013).
27. Kumar, N. *et al.* Second harmonic microscopy of monolayer MoS_2. *Phys. Rev. B* **87**, 161403(R) (2013).
28. Malard, L. M. *et al.* Observation of intense second harmonic generation from MoS_2 atomic crystals. *Phys. Rev. B* **87**, 207401(R) (2013).
29. Zeng, H. *et al.* Optical signature of symmetry variations and spin–valley coupling in atomically thin tungsten dichalcogenides. *Sci. Rep.* **3**, 1608 (2013).
30. Bistritzer, R. & MacDonald, A. H. Moiré bands in twisted double-layer graphene. *Proc. Natl Acad. Sci. USA* **108**, 12233–12237 (2011).
31. Sato, K. *et al.* Zone folding effect in Raman G-band intensity of twisted bilayer graphene. *Phys. Rev. B* **86**, 125414 (2012).
32. Kim, K. *et al.* Multiply folded graphene. *Phys. Rev. B* **83**, 235433 (2011).
33. Liu, W-T. & Shen, Y. R. Surface vibrational modes of α-quartz(0001) probed by sum-frequency spectroscopy. *Phys. Rev. Lett.* **101**, 016101 (2008).

Author contributions

S.W.W. and W.T.L. designed the project and prepared the manuscript. T.J. prepared the sample and performed the measurements. H.R.L. and X.G.G. carried out the *ab initio* calculation. D.H., S.Z. and Y.G.L. built the low-temperature experimental set-up. All authors contributed to analysis of the results and writing the manuscript.

Additional information

Supplementary information is available in the online version of the paper. Reprints and permissions information is available online at www.nature.com/reprints. Correspondence and requests for materials should be addressed to X.G.G., W.T.L. and S.W.W.

Competing financial interests

The authors declare no competing financial interests.